DNA/Fusogenic Lipid Nanocarrier Assembly: Millisecond Structural Dynamics

ARTICLE *in* JOURNAL OF PHYSICAL CHEMISTRY LETTERS · JUNE 2013

Impact Factor: 7.46 · DOI: 10.1021/jz400857z

9 AUTHORS, INCLUDING:

Angelina Angelova
Université Paris-Sud 11
88 PUBLICATIONS **1,679** CITATIONS
SEE PROFILE

Markus Drechsler
University of Bayreuth
196 PUBLICATIONS **6,746** CITATIONS
SEE PROFILE

Petr Stepanek
Academy of Sciences of the Czech Republic
170 PUBLICATIONS **2,290** CITATIONS
SEE PROFILE

Patrick Couvreur
Université Paris-Sud 11
588 PUBLICATIONS **25,870** CITATIONS
SEE PROFILE

THE JOURNAL OF PHYSICAL CHEMISTRY Letters

Letter

pubs.acs.org/JPCL

DNA/Fusogenic Lipid Nanocarrier Assembly: Millisecond Structural Dynamics

Borislav Angelov,[†] Angelina Angelova,*[,‡] Sergey K. Filippov,[†] Theyencheri Narayanan,[§] Markus Drechsler,[⊥] Petr Štěpánek,[†] Patrick Couvreur,[‡] and Sylviane Lesieur[‡]

[†]Institute of Macromolecular Chemistry, Academy of Sciences of the Czech Republic, CZ-16206 Prague, Czech Republic

[‡]CNRS UMR8612 Institut Galien Paris-Sud, Univ Paris Sud 11, F-92296 Châtenay-Malabry, France

[§]European Synchrotron Radiation Facility (ESRF), 6 rue Jules Horowitz, F-38043 Grenoble, France

[⊥]Laboratory for Soft Matter Electron Microscopy, Bayreuth Institute of Macromolecular Research, University of Bayreuth, D-95440 Bayreuth, Germany

S *Supporting Information*

ABSTRACT: Structural changes occurring on a millisecond time scale during uptake of DNA by cationic lipid nanocarriers are monitored by time-resolved small-angle X-ray scattering (SAXS) coupled to a rapid-mixing stopped-flow technique. Nanoparticles (NPs) of nanochannel organization are formed by PEGylation, hydration, and dispersion of a lipid film of the fusogenic lipid monoolein in a mixture with positively charged (DOMA) and PEGylated (DOPE-PEG$_{2000}$) amphiphiles and are characterized by the inner cubic structure of very large nanochannels favorable for DNA upload. Ultrafast structural dynamics of complexation and assembly of these cubosome particles with neurotrophic plasmid DNA (pDNA) is revealed thanks to the high brightness of the employed synchrotron X-ray beam. The rate constant of the pDNA/lipid NP complexation is estimated from dynamic roentgenograms recorded at 4 ms time resolution. pDNA upload into the vastly hydrated channels of the cubosome carriers leads to a fast nanoparticle−nanoparticle structural transition and lipoplex formation involving tightly packed pDNA.

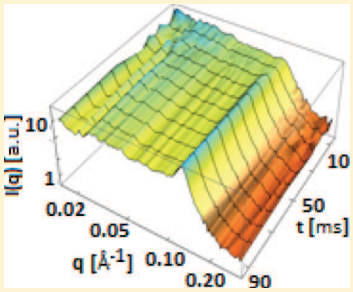

SECTION: Biomaterials, Surfactants, and Membranes

Studies of structure and stability of lipid/DNA complexes (lipoplexes)[1−17] are of ongoing interest for the success of prospective nanoparticle-based gene therapies. In this field, small-angle X-ray scattering (SAXS) has been recognized as a powerful structural technique for the design of DNA and drug carrier systems.[3,18−28] In a pioneering work, Lindman and colleagues[6] have stressed that the mechanism governing the lipoplex formation has not been understood yet due to the lack of information on the kinetics. Toward that aim, stopped-flow turbidity, fluorescence, and small-angle neutron scattering (SANS) have been employed to study the kinetics of salmon sperm DNA/liposome complex formation.[7] SANS measurements have established intermediate cylindrical structures, formed from liposomes on the time scale of seconds, and multilamellar aggregates grown on the time scale of minutes.[7] However, fluorescence and turbidity measurements have shown the necessity of elucidating the nanostructures forming on the shorter time scales.[6] Therefore, the in-depth understanding of the DNA/lipid nanoparticle (NP) assembly mechanism and kinetic pathways requires micro- and millisecond time-resolved structural investigations performed at state-of-the-art X-ray sources.[29−31]

Here, we report rapid-mixing stopped-flow SAXS investigation, on the millisecond time scale, of the assembly and complexation between neurotrophin-encoding plasmid DNA (pDNA) and fusogenic lipid carriers with nanochannelled organization (cubosome nanoparticles). It is considered that cubic NPs, built up by nonphospholipid molecules of a nonlamellar propensity (such as the fusogenic lipid monoolein, MO),[32−36] can mimic the structural and transport properties of certain porous icosahedral virion particles (see Figure 1S, Supporting Information). The controlled NP formulation with pDNA, using millisecond microfluidic mixing,[37] is anticipated to overcome the problems related to broad size distribution, physical instability, heterogeneous membrane structures, and rigid bulky aggregate formation observed with lipoplexes.[14,17] The kinetics of cubic membrane particle/pDNA complexation, enlightening a millisecond-range nanoparticle−nanoparticle structural transition, has not been previously investigated. The presented methodology for real time monitoring of the pDNA/lipid NP assembly offers a new approach for determination of the rate constants of the complexation from micro- and millisecond time-resolved roentgenograms.

PEGylated nanoparticles with nonlamellar inner-membrane organization and open nanochannels were prepared by hydration and dispersion of a mixed lipid film containing the

Received: April 23, 2013
Accepted: May 21, 2013
Published: May 28, 2013

fusogenic lipid MO, the cationic lipid dioctadecyldimethylammonium bromide (DOMA), and the PEGylated lipid 1,2-dioleoyl-*sn*-glycero-3-phospho-ethanolamine-*N*-(methoxy-(polyethyleneglycol)-2000) ammonium salt (DOPE-PEG$_{2000}$). The dispersed NPs were characterized by means of SAXS (Figure 1a) and quasi-elastic light scattering (Figure 2S, Supporting Information). After establishing the structural organization of the MO-based cationic NPs, we monitored the kinetic pathway of their assembly with pDNA (Figure 1b) by SAXS with 4 ms time resolution (Figure 2) and the structural transformations involving the earliest stages of the pDNA condensation and packing into the nanocarriers.

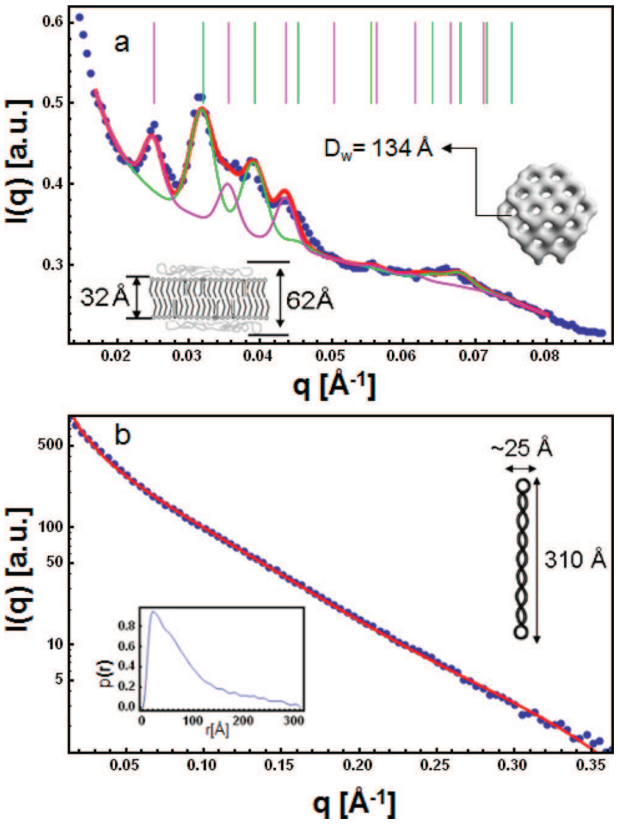

Figure 1. (a) Steady-state SAXS curve of PEGylated cationic cubosome NPs formed by the MO/DOMA/DOPE-PEG$_{2000}$ (82/15/3 mol %) mixture in excess buffer medium. The pink fitting curve and the pink bars denote, from left to right, the (110), (200), (211), (220), (310), (222), (321), and (400) reflections of a primitive cubic lattice *Im*3*m* (Q^{229}), whereas the green curve and bars mark the (110), (111), (200), (211), (220), (221), (310), and (222) reflections of a double diamond cubic lattice structure *Pn*3*m* (Q^{224}). (Inset) Dimensions of the lipid bilayer and water nanochannels (D_w) in the cubosome NPs obtained from the performed fit. (b) Steady-state SAXS pattern of the studied plasmid DNA and a performed fit by a core/shell cylinder model. The corresponding pair distance distribution function is shown in the inset.

The Bragg peaks, resolved in the SAXS pattern presented in Figure 1a, give evidence for the liquid-crystalline (LC) internal structure of the blank lipid particles prior to pDNA loading. The recorded NP scattering profile differs from monotonically vanishing oscillations of monodisperse vesicle scattering.[30] Considering the possible symmetries,[21,38−40] a best fit was obtained with coexisting NPs of *Pn*3*m* and *Im*3*m* inner cubic symmetries. According to the phase diagram of the MO/water system,[33] gyroid (*Ia*3*d*) cubic structures cannot exist in excess aqueous phase (i.e., under conditions required for NP dispersion).

The SAXS data indicate that stable cationic cubic NPs could be of *Pn*3*m* or *Im*3*m* inner cubic structures, similar to the noncharged LC systems.[38,39] The derived cubic lattice parameters are $a_{(Pn3m)}$ = 27.7 nm and $a_{(Im3m)}$ = 35.3 nm, respectively. These structural results reveal larger aqueous nanochannels in the positively charged cubosome NPs as compared to the those in the bulk cubic phase of fully hydrated MO[34] ($a_{(Pn3m)}$ = 10.5 nm). This suggests a higher loading capacity for pDNA (or large-size therapeutic proteins) in the swollen nanochannels with cubic packing. In biological systems, highly hydrated natural cubic membranes of mitochondria (channel size > 50 nm) have enabled significant oligonucleotide uptake.[41]

Stopped-flow rapid mixing coupled to SAXS was performed at a constant lipid NP concentration and varying pDNA loadings (see the full description of the experimental procedure in the Supporting Information). The SAXS curves recorded with 4 ms time resolution are presented in Figure 2. They reveal the millisecond-lived intermediate states of the pDNA/lipid NP assembly kinetics pathway. A structural transition from cubosome (MO/DOMA/DOPE-PEG$_{2000}$) particles to a new supramolecular structure, formed by the lipid/pDNA complexes, was detected throughout the first 10−90 ms from the onset of the in-situ-monitored complexation process.

Generally, the lipoplex assembly kinetics involves at least three stages, (i) a very fast process of DNA charge neutralization (rate constant k_1), (ii) intermediate formation and condensation of many neutralized DNA molecules (at charge neutralization degree above 80%) into pDNA/lipid assemblies (rate constant k_2), and (iii) slow relaxation and rearrangement of the generated complexes into more ordered or aggregated states (rate constant k_3). Under the investigated conditions of excess concentration of lipid carriers with respect to DNA plasmids, the kinetics of the pDNA/cationic lipid NP assembly is initially determined by the variation of the chemical potential of the negatively charged pDNA available for complexation with positively charged NPs. Assuming that the NPs are of homogeneously distributed charges, every elementary charge (−1e) on the pDNA macroion is neutralized by a lipid head group charge (+1e). The kinetics of the initial pDNA charge neutralization process for different rate constants k_1 is provided in Figure 3S (Supporting Information).

The condensation of many pDNA molecules in the cationic nanocarriers begins above a critical degree of charge neutralization assuming a random sequential adsorption[42] for pDNA. This gives rise to "stage 2" of the pDNA/NP assembly kinetics resulting in the appearance of a Bragg diffraction peak (Figure 2). The increasing Bragg peak at $q \approx 0.125$ Å (d spacing, $d \approx 5$ nm), accompanied by decreasing peaks of a cubic lattice, reveals a cubic-to-stacked bilayer structure transformation in the nanoparticulate system (Figures 2b and 3). It can be suggested that the cylindrical aqueous nanochannels of cubic packing serve as a predefined template for pDNA intercalation and condensation. pDNA, adsorbed on the oppositely charged surface of the swollen nanochannels in the cubic membrane carriers, provokes the nanochannels' collapse. Thus, the second stage of the kinetics, revealed on the time scale of milliseconds, corresponds to the formation of intermediates, in which the secondary structure of pDNA

dx.doi.org/10.1021/jz400857z | *J. Phys. Chem. Lett.* 2013, 4, 1959−1964

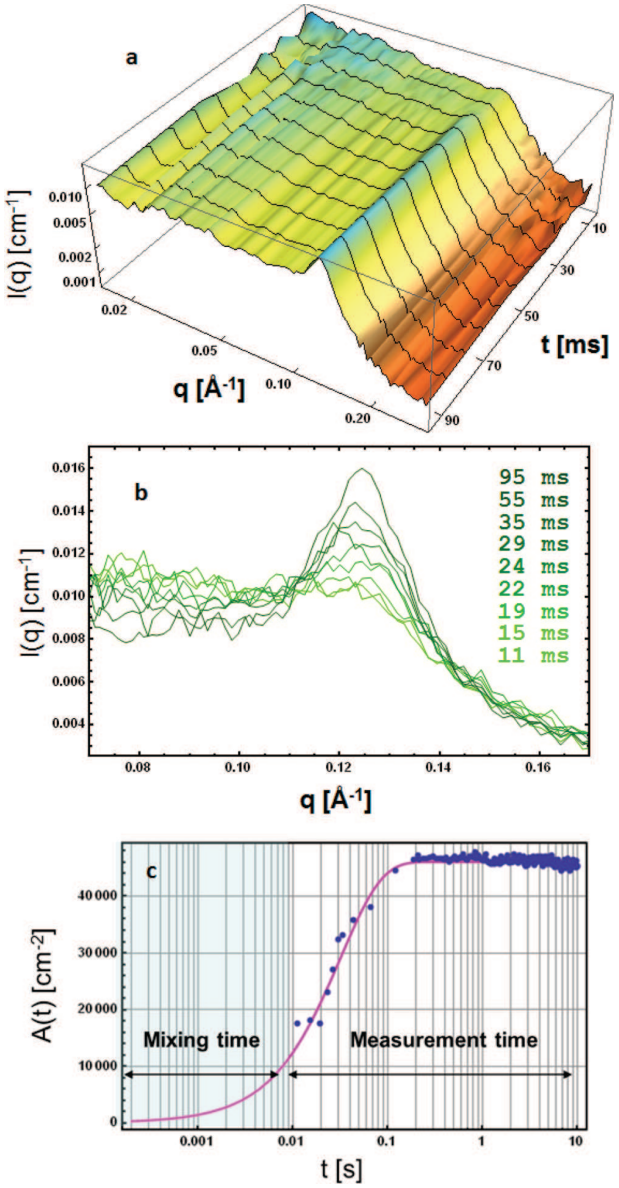

Figure 2. (a) Millisecond-range kinetic pathway of the pDNA/cationic lipid NP assembly revealed by time-resolved SAXS (4 ms exposure time), coupled to stopped-flow rapid mixing and allowing for real time monitoring of the complexes' formation between pDNA and nanochannel-type fusogenic lipid carriers. The lipid NPs and pDNA (encoding for the neurotrophin BDNF) are those from Figure 1. (b) Initial kinetic frames for nine consecutive shots of stopped-flow rapid mixing presenting the time evolution of the Bragg peak (q = 0.125 Å) during in situ formation of complexes in the MO/DOMA/DOPE-PEG_{2000}/pDNA NP system. (c) Fitting of the kinetic dependence of the experimental Bragg peak areas, $A(t)$, using eq 1. The incident X-ray flux for this time-resolved study of fast structural changes is 4.7×10^{13} photons/s.

becomes more compact. The pDNA condensation is confirmed also by a cryo-TEM image (see Figure 4b below).

The d spacing values suggest confinement of the supercoiled pDNA in particles of weakly ordered bilayer structures. The lack of a second-order Bragg peak of a multilamellar structure implies that the number of ordered lamellas, formed upon rapid mixing, and the lipoplex NP sizes are small. Following the initial

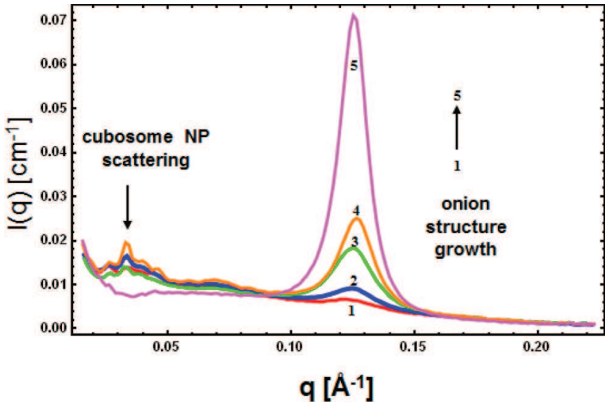

Figure 3. Role of the cationic lipid/pDNA charge ratio for the pDNA compaction and assembly in fusogenic lipid NPs. Steady-state SAXS patterns recorded after rapid mixing of equal volumes of PEGylated cationic lipid NPs (MO/DOMA/DOPE-PEG_{2000} 82/15/3 mol %) and pDNA (BDNF) solutions at charge ratios, $Z_{\pm}$, varying in the sequence 16.3 (1), 7.4 (2), 3.7 (3), 2.6 (4), and 1.6 (5).

growth, the Bragg peak intensity reaches a steady-state level after approximately 95 ms (Figure 2c). Simultaneously, the full width at half-maximum (fwhm) of the scattering peak decreases with time and reaches a constant value. This reveals a structural transformation over milliseconds rather than over seconds or minutes.[7]

Figure 2c shows the millisecond time dependence of the Bragg peak area, $A(t)$, characterizing the kinetics of lipoplex formation upon pDNA assembly with the positively charged cubic lipid NPs. The two regimes observed, namely, (i) the kinetic regime where the peak area evolves with time and (ii) the steady-state regime, can be assigned respectively to stage 2 (condensation step) and stage 3 (relaxation step) of the complexation. The fact that no further changes (beyond 95 ms) in the area of the Bragg peak were observed over time indicates that the internal structure relaxation of the complexes (stage 3 of the pathway) is very slow for a time-resolved SAXS experiment. The rate constant, $k_2 \approx 30\ s^{-1}$, determined from the time dependence of the Bragg peak area, is found to be considerably higher than that reported[6] for spherical liposomes, $k_2 \approx 0.6\ s^{-1}$.

A sigmoid rising function (eq 1) was used for fitting of the time sequence of intermediate states corresponding to the pathway of pDNA/lipid NP complexation (Figure 2c). The experimentally measured area of the Bragg peak, $A(t)$, is proportional to the concentration of the rapidly forming pDNA/lipid assemblies

$$A(t) = A_{max}(1 - e^{-k_2 t}) \quad (1)$$

where A_{max} is the maximal peak area, k_2 is a rate constant analogous to a first-order chemical reaction constant, and t is the time. The plateau of $A(t)$ confirms that the concentration of the pDNA/lipid assemblies increases with time until reaching a maximum value. In a diffusion-limited reaction kinetics, the system reaches a plateau in the time dependence of its free energy (stage 3 of the complexation kinetics) when the pDNA/cationic lipid complex is fully formed. This is best described by lipoplex assembly kinetics over the millisecond time scale. The rate constant, $k_2 = 31.36\ s^{-1}$, is the single fitting parameter in eq 1. Quantitatively, it indicates that the fusogenic lipid/pDNA assemblies form 50 times faster than those of previously studied

dx.doi.org/10.1021/jz400857z | J. Phys. Chem. Lett. 2013, 4, 1959−1964

lipoplexes of liposome-forming lipids.[7] Therefore, we would like to emphasize that this is the fastest kinetics ever reported for the pDNA/lipid complexes' formation structural pathway.

The steady-state SAXS intensity plots characterizing the uptake of pDNA into the highly hydrated fusogenic lipid NPs and the corresponding lipoplex formation are presented in Figure 3 as a function of the cationic lipid/pDNA charge ratio ($Z_{\pm}$). At a constant concentration of PEGylated cationic lipid NPs (providing excess positive charges in the system), the complex formation is governed by the concentration of the DNA charges determining the charge ratio $Z_{\pm}$ ($Z_{\pm}$ is defined as the molar ratio between the positively charged ammonium head groups present in the lipid NPs and the negatively charged phosphate groups of pDNA).

Figure 3 shows that the intensity, specifically the integral area, of the Bragg diffraction peak at $q \approx 0.125$ Å increases with the amount of pDNA assembled with cationic nanocarriers after condensation. Loading of pDNA into the swollen channels of the cubosome NPs, accompanied by essential DNA charge neutralization and dehydration, transforms the cubic membrane particles into structures of a new packing. An increasing Bragg peak intensity (from pattern 1 to pattern 5) indicates a better ordered inner structure of the compacted pDNA/lipid particles and a bigger number of stacked bilayers in the nanoparticulate complexes. While the Bragg peak, evidencing the lipid/pDNA complex formation, increases in intensity as a function of the pDNA concentration (Figure 3), the scattering of the cubosome NPs (at $q < 0.08$ Å) vanishes upon pDNA loading. The cubosomal scattering is absent for maximal pDNA concentration (Figure 3, curve 5). A similar decrease of the cubosomal scattering is observed over time in Figure 2. Table 1S (Supporting Information) presents the estimated inner lamellar periodicity of the lipid/pDNA complexes, $d \approx 5$ nm, which appears to be invariant of the charge ratio, $Z_{\pm}$.

Figure 4a proposes a scheme of the lipid cubic NP/pDNA assembly pathway involving a cubic membrane-to-stacked bilayer structural transition. The adsorption of negatively charged pDNA at the cationic cubosome surfaces (stage 1) creates asymmetric configurations at the lipid membrane/water interfaces. The bound supercoiled pDNA may affect the hydration, curvature, and elasticity of the lipid bilayers. As a result, the cubic lipid membrane is deformed and is rapidly transformed into a small curvature assembly. The developing onion-like inner organization encapsulates pDNA in an intercalated state (stage 2 of the pathway).

Here, the suggested scheme (Figure 4a) involves a continuous, low-energy cubic membrane-to-weakly ordered onion bilayer transition mechanism.[31] At variance with the liposome-forming lamellar lipids,[4] this mechanism does not involve harsh splitting of the bicontinuous lipid membrane and of the lipid/water interfaces upon formation of complexes with DNA. The MO-based cubosomic carriers (Figure 1) are characterized by an intrinsic membrane curvature that is absent in the previously studied liposomes.[4,7] For lamellar-phase lipids, vesicle rupture appears to be a major step before a sandwich lipoplex formation with DNA. According to Huebner et al.,[4] the complex formation is associated with vesicle aggregation, rupture, and opening of the lipid bilayers. After mixing with DNA, the DNA-coated unilamellar vesicles are deformed and clustered. These clusters have been considered as intermediates in the formation of multilamellar complexes.

In our case, the pDNA complexation with nanochannelled lipid carriers induces transformation of the inner cubic NP

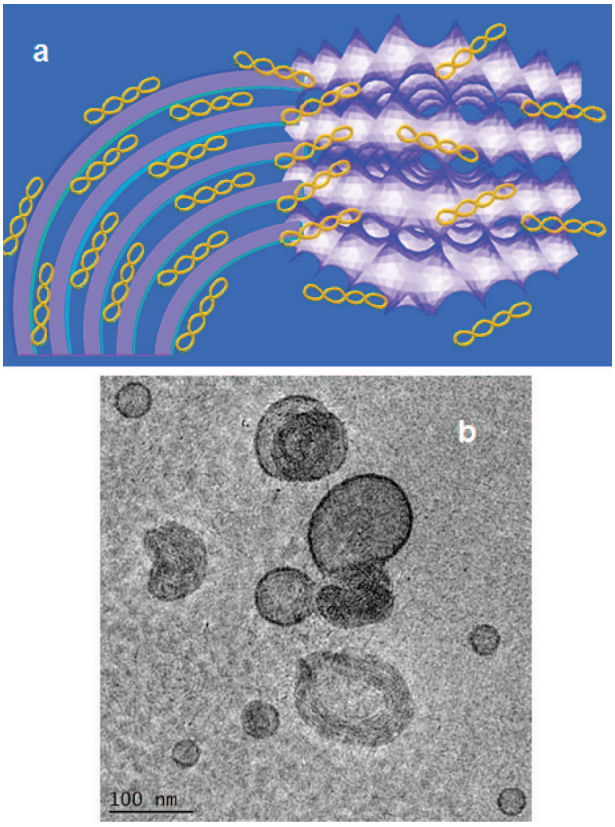

Figure 4. Pathway of pDNA confinement in highly hydrated nanochannelled carriers. (a) Cartoon representation of the transient states upon pDNA condensation in a diamond-type cubic membrane nanocarrier and building up of a structure from aligned lipid bilayers. The intercalation of the supercoiled pDNA in the lipid carrier causes a cubic membrane-to-stacked bilayer transition. (b) Cryo-TEM image of the generated MO/DOMA/DOPE-PEG_{2000}/pDNA lipoplex particles.

structure to a structure of aligned bilayers (Figure 4). The process occurs considerably faster than the vesicle rupture/multilamellar lipoplex assembly from bilayer fragments.[4] Actually, the intermediate structures with large aqueous channels,[40] necessary for the cubic-to-lamellar transition,[31] are already present in the studied dynamic system of NPs (Figure 1a). In terms of free energy, the structural intermediates with very large water channels are far from an equilibrium state (deep energy minimum) and may easily undergo transformations associated with low-energy barriers. Therefore, owing to the nonequilibrium nature of the highly hydrated cationic cubic NPs, the kinetic pathway reported here appears to be essentially accelerated with regard to equilibrium lamellar-to-lipoplex and inverted hexagonal-to-multilamellar lipoplex transition pathways related to high-energy barriers (specifically slow kinetics over several minutes).

Figure 4b shows a cryo-TEM image of the cationic NP/pDNA assembly. The high-intrinsic-curvature lipid (MO), in combination with PEGylation of the membrane, seems to favor smaller-size NP formation as compared to other lipid transfection types, for which lipoplexes of up to 2−5 μm have been reported (the so-called giant lipoplexes).[13] Here, massive clustering and fusion into large lipid/pDNA complexes appear to be hampered by the PEGylated NP surface, which provides steric stabilization.[11] The cryo-TEM results confirm

that the lipid membrane NPs with open-channel architectures are transformed upon pDNA loading into densely packed structures. The resulting inner NP packing is similar to that in some double-stranded DNA bacteriophage particles.[5]

In conclusion, pDNA-induced millisecond structural dynamic changes of synthetic cubic membrane lipid nanocarriers were cinematographed by time-resolved synchrotron SAXS coupled to a rapid-mixing stopped-flow technique. The obtained results evidenced that the phase transformation kinetics in the NP systems is influenced by the geometry of the lipid/water interfaces, their charge, and hydration. They demonstrated the role of the highly hydrated nanochannel structure of the cationic nanocarriers for the kinetics of the pDNA uptake. The investigated NPs completely rearranged their inner cubic membrane architecture upon loading of the plasmids in less than 150 ms, and as an outcome, fully condensed pDNA was obtained over the subsecond time scales. The 4 ms time resolution of the SAXS experiments allowed access of the earliest structural moieties and collection of quantitative structural information about the fusogenic lipid NP/pDNA complexation process. The ultrastructures promoting millisecond dynamics in the membrane transformations were established. These dynamic intermediates, formed at energy states that are far from the energetic minimum for an equilibrium system, may be markedly more favorable for performing gene transfer processes across cell membranes (i.e., low-energy consumption and rapid kinetics of geometry transformations) as compared to the equilibrium lamellar and hexagonal structures (studied previously by SAXS), which require prolonged incubation with living cells in transfection assays. Therefore, the physicochemical knowledge obtained from the proposed methodology for real time control of the ultrastructures occurring on the time scale of pDNA-induced nanoparticle−nanoparticle structural transitions is expected to contribute to the development of novel gene carriers as well as to be applied for elucidation of assembly pathways in various biomolecular and NP systems.

EXPERIMENTAL METHODS

Small-angle X-ray scattering experiments, coupled to a rapid-mixing stopped-flow device, were performed at the ID02 beamline[29] of the European Synchrotron Radiation Facility (ESRF, Grenoble, France). A high-sensitivity low-noise CCD detector (FReLoN 4M) was employed for time-resolved structural studies. The high X-ray brightness available at the ID02 beamline provided optimal flux (4.7×10^{13} photons/s) to investigate the kinetics of millisecond structural transformations without sample destruction. The stopped-flow rapid-mixing technique permitted precise control over the mixing conditions via the turbulent mixing, variable flow rate, and small mixing volumes of PEGylated lipid NPs and pDNA solutions. The SAXS patterns were integrated over 4 ms. Time-resolved SAXS on the 4 ms time scale is at the forefront border of fast kinetic structural measurements feasible with nanomedicine materials. The rate constant of the pDNA/lipid NP assembly kinetics was determined by fitting of about 750 SAXS patterns. Cryogenic transmission electron microscopy (cryo-TEM) studies were performed using a Zeiss EM922 Omega energy-filtered TEM (EFTEM) instrument (Zeiss NTS GmbH, Germany) equipped with pertinent devices (Zeiss cryobox and cryo transfer holder, Gatan, Germany). Quasi-elastic light scattering investigation of the NPs' sizes was performed by a Nanosizer apparatus Nano-ZS90 (Malvern, France).

ASSOCIATED CONTENT

Supporting Information

Supplementary results (Figures 1S−4S, Table 1S), showing biomimetism relating a virion capsid particle and a cubic lipid nanoparticle, the particle size distribution in a MO/DOMA/DOPE-PEG_{2000} dispersed system, kinetics of charge neutralization, the hydrodynamic diameter, and repeat spacing characterizing complexes formed at different charge ratios for varying concentrations along with the full methods description. This material is available free of charge via the Internet at http://pubs.acs.org.

AUTHOR INFORMATION

Corresponding Author

*E-mail: Angelina.Angelova@u-psud.fr.

Notes

The authors declare no competing financial interest.

ACKNOWLEDGMENTS

The ESRF is thanked for granting SAXS beam time and user support to the Project SC-3358 at the ID02 beamline. B.A. acknowledges the Czech Science Foundation Grant No. P208/10/1600. A.A. and S.L. acknowledge the Program ANR SIMI10 Nanosciences and LabEx LERMIT. M.D. acknowledges the support from BIMF (Bayreuth Institute of Macromolecular Research) and BZKG (Bayreuth Center for Colloids and Interfaces).

REFERENCES

(1) Tresset, G.; Lansac, Y. Long-Range Architecture of Single Lipid-Based Complex Nanoparticles with Local Hexagonal Packing. *J. Phys. Chem. Lett.* **2011**, *2*, 41−46.

(2) Gustafsson, J.; Arvidson, G.; Karlsson, G.; Almgren, M. Complexes between Cationic Liposomes and DNA Vizualized by Cryo-TEM. *Biochim. Biophys. Acta* **1995**, *1235*, 305−312.

(3) Caracciolo, G.; Pozzi, D.; Caminiti, R.; Marchini, C.; Montani, M.; Amici, A.; Amenitsch, H. Enhanced Transfection Efficiency of Multicomponent Lipoplexes in the Regime of Optimal Membrane Charge Density. *J. Phys. Chem. B* **2008**, *112*, 11298−11304.

(4) Huebner, S.; Battersby, B. J.; Grimm, R.; Cevc, G. Lipid−DNA Complex Formation: Reorganization and Rupture of Lipid Vesicles in the Presence of DNA as Observed by Cryoelectron Microscopy. *Biophys. J.* **1999**, *76*, 3158−3166.

(5) Schmutz, M.; Durand, D.; Debin, A.; Palvadeau, Y.; Etienne, A.; Thierry, A. R. DNA Packing in Stable Lipid Complexes Designed for Gene Transfer Imitates DNA Compaction in Bacteriophage. *Proc. Nat. Acad. Sci. U.S.A.* **1999**, *96*, 12293−12298.

(6) Barreleiro, P. C.; Lindman, B. The Kinetics of DNA−Cationic Vesicle Complex Formation. *J. Phys. Chem. B* **2003**, *107*, 6208−6213.

(7) Barreleiro, P. C. A.; May, R. P.; Lindman, B. Mechanism of Formation of DNA−Cationic Vesicle Complexes. *Faraday Discuss.* **2002**, *122*, 191−201.

(8) Guo, X.; Huang, L. Recent Advances in Nonviral Vectors for Gene Delivery. *Acc. Chem. Res.* **2012**, *45*, 971−979.

(9) Nguyen, J.; Szoka, F. C. Nucleic Acid Delivery: The Missing Pieces of the Puzzle? *Acc. Chem. Res.* **2012**, *45*, 1153−1162.

(10) Zelphati, O.; Nguyen, C.; Ferrari, M.; Felgner, J.; Tsai, Y.; Felgner, P. L. Stable and Monodisperse Lipoplex Formulations for Gene Delivery. *Gene Ther.* **1998**, *5*, 1272−1282.

(11) Wheeler, J. J.; Palmer, L.; Ossanlou, M.; MacLachlan, I.; Graham, R. W.; Zhang, Y. P.; Hope, M. J.; Scherrer, P.; Cullis, P. R. Stabilized Plasmid−Lipid Particles: Construction and Characterization. *Gene Ther.* **1999**, *6*, 271−281.

(12) Hafez, I. M.; Cullis, P. R. Roles of Lipid Polymorphism in Intracellular Delivery. *Adv. Drug Delivery Rev.* **2001**, *47*, 139−148.

(13) Tarahovsky, Y. S. Cell Transfection by DNA−Lipid Complexes — Lipoplexes. *Biochemistry (Moscow)* **2009**, *74*, 1293−1304.
(14) Bally, M. B.; Zhang, Y.-P.; Wong, F. M. P.; Kong, S.; Wasan, E.; Reimer, D. L. Lipid/DNA Complexes as an Intermediate in the Preparation of Particles for Gene Transfer: An Alternative to Cationic Liposome/DNA Aggregates. *Adv. Drug Delivery Rev.* **1997**, *24*, 275−290.
(15) Angelov, B.; Angelova, A.; Filippov, S.; Karlsson, G.; Terrill, N.; Lesieur, S.; Štěpánek, P. Topology and Internal Structure of PEGylated Lipid Nanocarriers for Neuronal Transfection: Synchrotron Radiation SAXS and Cryo-TEM Studies. *Soft Matter* **2011**, *7*, 9714−9720.
(16) Ma, B.; Zhang, S.; Jiang, H.; Zhao, B.; Lv, H. Lipoplex Morphologies and Their Influences on Transfection Efficiency in Gene Gelivery. *J. Controlled Release* **2007**, *123*, 184−194.
(17) Massotti, A.; Mossa, G.; Cametti, C.; Orgaggi, G.; Bianco, A.; Del Grosso, N.; Malizia, D.; Esposito, C. Comparison of Different Commercially Available Cationic Liposome−DNA Lipoplexes: Parameters Influencing Toxicity and Transfection Efficiency. *Colloids Surf. B* **2009**, *68*, 136−144.
(18) McLoughlin, D.; Imperor-Clerc, M.; Langevin, D. A New Cubic Phase Containing DNA and Surfactant. *ChemPhysChem* **2004**, *5*, 1619−1629.
(19) Angelova, A.; Angelov, B.; Garamus, V. M.; Couvreur, P.; Lesieur, S. Small-Angle X-ray Scattering Investigations of Biomolecular Confinement, Loading, and Release from Liquid-Crystalline Nanochannel Assemblies. *J. Phys. Chem. Lett.* **2012**, *3*, 445−457.
(20) Yaghmur, A.; Laggner, P.; Sartori, B.; Rappolt, M. Calcium Triggered L_α−H_2 Phase Transition Monitored by Combined Rapid Mixing and Time-Resolved Synchrotron SAXS. *PloS ONE* **2008**, *3*, e2072.
(21) Angelov, B.; Angelova, A.; Ollivon, M.; Bourgaux, C.; Capitelli, A. Diamond-Type Lipid Cubic Phase with Large Water Channels. *J. Am. Chem. Soc.* **2003**, *125*, 7188−7189.
(22) Yaghmur, A.; Rappolt, M. Structural Characterization of Lipidic Systems under Nonequilibrium Conditions. *Eur. Biophys. J.* **2012**, *41*, 831−840.
(23) Angelov, B.; Angelova, A.; Garamus, V. M.; Le Bas, G.; Lesieur, S.; Ollivon, M.; Funari, S. S.; Willumeit, R.; Couvreur, P. Small-Angle Neutron and X-ray Scattering from Amphiphilic Stimuli-Responsive Diamond-Type Bicontinuous Cubic Phase. *J. Am. Chem. Soc.* **2007**, *129*, 13474−13479.
(24) Angelov, B.; Angelova, A.; Vainio, U.; Garamus, V. M.; Lesieur, S.; Willumeit, R.; Couvreur, P. Long-Living Intermediates during a Lamellar to a Diamond-Cubic Lipid Phase Transition: A Small-Angle X-ray Scattering Investigation. *Langmuir* **2009**, *25*, 3734−3742.
(25) Dong, Y.-D.; Tilley, A. J.; Larson, I.; Lawrance, M. J.; Amenitsch, H.; Rappolt, M.; Hanley, T.; Boyd, B. J. Nonequilibrium Effects in Self-Assembled Mesophase Materials: Unexpected Supercooling Effects for Cubosomes and Hexosomes. *Langmuir* **2010**, *26*, 9000−9010.
(26) Angelov, B.; Angelova, A.; Mutafchieva, R.; Lesieur, S.; Vainio, U.; Garamus, V. M.; Jensen, G. V.; Pedersen, J. S. SAXS Investigation of a Cubic to a Sponge (L_3) Phase Transition in Self-Assembled Lipid Nanocarriers. *Phys. Chem. Chem. Phys.* **2011**, *13*, 3073−3081.
(27) Saveyn, P.; van der Meeren, P.; Zackrisson, M.; Narayanan, T.; Olsson, U. Subgel Transition in Diluted Vesicular DODAB Dispersions. *Soft Matter* **2009**, *5*, 1735−1742.
(28) Narayanan, T. High Brilliance Small-Angle X-ray Scattering Applied to Soft Matter. *Curr. Opin. Colloid Interface Sci.* **2009**, *14*, 409−415.
(29) Panine, P.; Finet, S.; Weiss, T. M.; Narayanan, T. Probing Fast Kinetics in Complex Fluids by Combined Rapid Mixing and Small-Angle X-ray Scattering. *Adv. Colloid Interface Sci.* **2006**, *127*, 9−18.
(30) Gummel, J.; Sztucki, M.; Narayanan, T.; Gradzielski, M. Concentration Dependent Pathways in Spontaneous Self-Assembly of Unilamellar Vesicles. *Soft Matter* **2011**, *7*, 5731−5738.
(31) Conn, C. E.; Ces, O.; Mulet, X.; Finet, S.; Winter, R.; Seddon, J. M.; Templer, R. H. Dynamics of Structural Transformations between Lamellar and Inverse Bicontinuous Cubic Lyotropic Phases. *Phys. Rev. Lett.* **2006**, *96*, 108102.
(32) Hyde, S. T.; Anderson, S.; Ericsson, B.; Larsson, K. A Cubic Structure Consisting of a Lipid Bilayer Forming an Infinite Periodic Minimal Surface of the Gyroid Type in the Glycerol Monooleate−Water System. *Z. Kristallogr.* **1984**, *168*, 213−219.
(33) Qiu, H.; Caffrey, M. The Phase Diagram of the Monoolein/Water System: Metastability and Equilibrium Aspects. *Biomaterials* **2000**, *21*, 223−234.
(34) Angelova, A.; Angelov, B.; Lesieur, S.; Mutafchieva, R.; Ollivon, M.; Bourgaux, C.; Willumeit, R.; Couvreur, P. Dynamic Control of Nanofluidic Channels in Protein Drug Delivery Vehicles. *J. Drug Delivery Sci. Technol.* **2008**, *18*, 41−45.
(35) Angelov, B.; Angelova, A.; Papahadjopoulos-Sternberg, B.; Hoffmann, S. V.; Nicolas, V.; Lesieur, S. Protein-Containing PEGylated Cubosomic Particles: Freeze-Fracture Electron Microscopy and Synchrotron Radiation Circular Dichroism Study. *J. Phys. Chem. B* **2012**, *116*, 7676−7686.
(36) Angelova, A.; Angelov, B.; Mutafchieva, R.; Lesieur, S.; Couvreur, P. Self-Assembled Multicompartment Liquid Crystalline Lipid Carriers for Protein, Peptide, and Nucleic Acid Drug Delivery. *Acc. Chem. Res.* **2011**, *44*, 147−156.
(37) Zhigaltsev, I. V.; Belliveau, N.; Hafez, I.; Leung, A. K. K.; Huft, J.; Hansen, C.; Cullis, P. R. Bottom-Up Design and Synthesis of Limit Size Lipid Nanoparticle Systems with Aqueous and Triglyceride Cores Using Millisecond Microfluidic Mixing. *Langmuir* **2012**, *28*, 3633−3640.
(38) Nakano, M.; Sugita, A.; Matsuoka, H.; Handa, T. Small Angle X-ray Scattering and ^{13}C NMR Investigation on the Internal Structure of "Cubosomes". *Langmuir* **2001**, *17*, 3917−3922.
(39) Nakano, M.; Teshigawara, T.; Sugita, A.; Leesajakul, W.; Taniguchi, A.; Kamo, T.; Matsuoka, H.; Handa, T. Dispersions of Liquid Crystalline Phases of the Monoolein/Oleic Acid/Pluronic F127 System. *Langmuir* **2002**, *18*, 9283−9288.
(40) Angelov, B.; Angelova, A.; Garamus, V. M.; Drechsler, M.; Willumeit, R.; Mutafchieva, R.; Štěpánek, P.; Lesieur, S. Earliest Stage of the Tetrahedral Nanochannel Formation in Cubosome Particles from Unilamellar Nanovesicles. *Langmuir* **2012**, *28*, 16647−16655.
(41) Almshergi, Z.; Hyde, S.; Ramachandran, M.; Deng, Y. Cubic Membranes: A Structure-Based Design for DNA Uptake. *J. R. Soc., Interface* **2008**, *5*, 1023−1029.
(42) Maltsev, E.; Wattis, J.; Byrne, H. DNA Charge Neutralization by Linear Polymers: Irreversible Binding. *Phys. Rev. E* **2006**, *74*, 011904.

Supporting Information

DNA/Fusogenic Lipid Nanocarrier Assembly: Millisecond Structural Dynamics

Borislav Angelov, Angelina Angelova*, Sergey K. Filippov, Theyencheri Narayanan, Markus Drechsler, Petr Štěpánek, Patrick Couvreur, Sylviane Lesieur

*E-mail: Angelina.Angelova@u-psud.fr

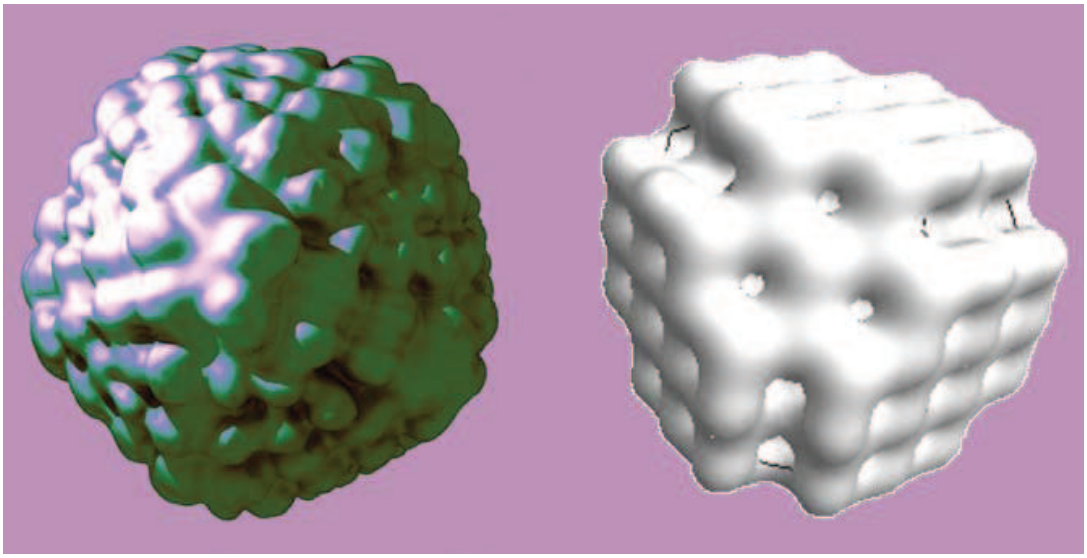

Figure 1S. Biomimetism relating a virion capsid particle (exemplified by the *Nudaurelia capensis omega virus*, PDB code: 1OHF [1,2]) (left) and a cubic lipid nanoparticle of a diamond type [3,4] (right). Both structures represent porous self-assembled objects that may adjust their surface-exposed nanopores and undergo structural transitions under applied external stimuli [1,3,4]. The latter can trigger release of entrapped molecules [5]. The similar sizes, surface topologies, and flexible channel organizations of these biomolecular-carrier systems could be exploited for challenging gene or drug delivery applications.

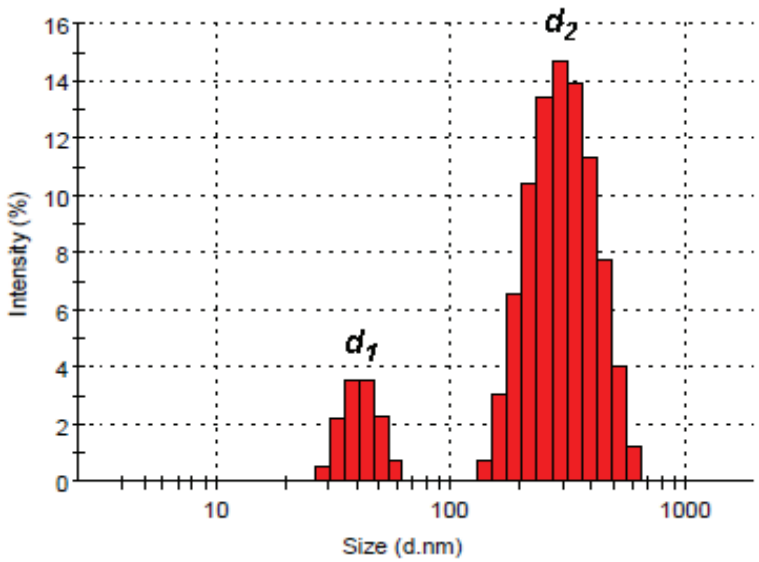

Figure 2S. Particle size distribution in a MO/DOMA/DOPE-PEG_{2000} (82/15/3 mol.%) dispersed lipid system established by quasi-elastic light scattering (QELS). The size statistics intensity plot shows two coexisting populations of nanoparrticles (NPs) with mean hydrodynamic diameters d_1= 41 nm (vesicular bilayers) and d_2 = 295 nm (cubosomes as revealed by SAXS in Fig. 1). Small vesicular membrane bilayer elements, present in a coexistence with the cubosome NPs, appear to be necessary [6,7] for the formation of stable cubosomes at ambient temperature.

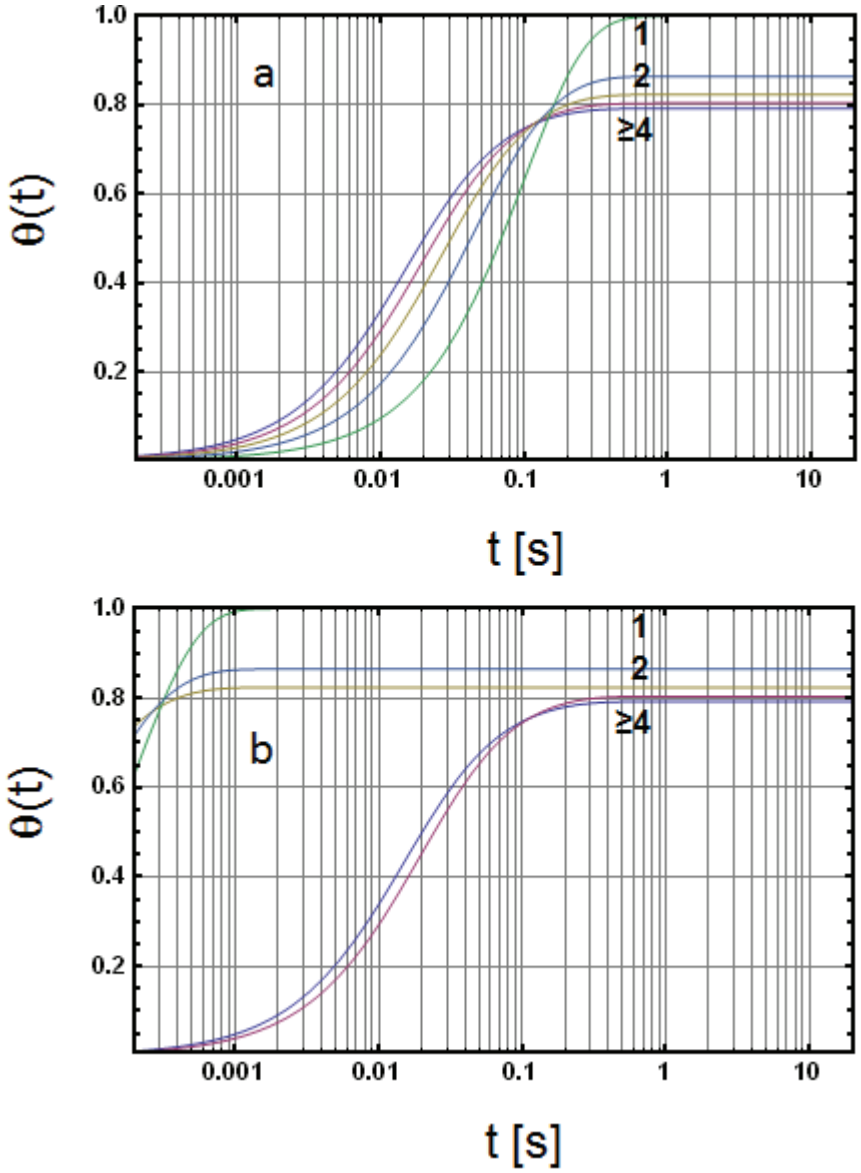

Figure 3S. Kinetics of charge neutralization, $\theta(t)$, calculated on the basis of a random sequential adsorption model (Eq. 20, Ref. 8) for binding rate constants $k_1 = 10\ s^{-1}$ (a) and $k_1 = 5000\ s^{-1}$ (b) at varying number of positive charges, n, per particle. The DNA molecule is of an infinite length in this model and the charge neutralization plateau is reached at $n \geq 4$ for $t \geq 0.1$ s.

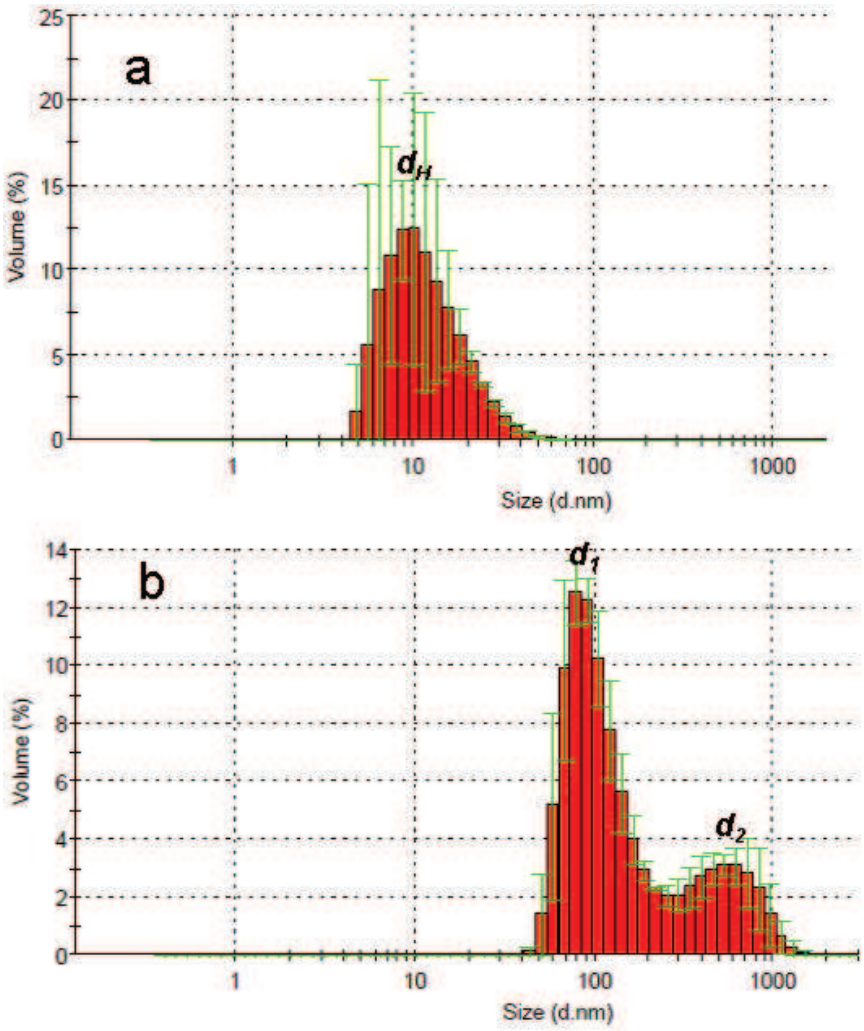

Figure 4S. Hydrodynamic diameter, d_H, of (a) fully hydrated supercoiled plasmid DNA (pDNA) encoding for human BDNF (d_H = 10.1 nm) and of (b) PEGylated cationic lipid MO/DOMA/DOPE-PEG_{2000}/pDNA complexes formed at a selected charge ratio $Z_{+/-}$. The volume size distribution is determined at temperature 25 ^{o}C. The NPs main fraction in (b) is centred at a hydrodynamic diameter d_1 = 79 nm, while a minor fraction of complexes is centred at a hydrodynamic size d_2 = 531nm. The error bars are given in green.

Table 1.

Repeat spacing, *d*, characterizing the PEGylated cationic-lipid-NP/pDNA (human BDNF) complexes formed at different cationic lipid/pDNA charge ratios ($Z_{+/-}$) for varying concentrations of the neurotrophic plasmid, C_{pDNA}, used for mixing. The head group charge of the cationic lipid DOMA is +1*e*.

C_{pDNA} [mg/mL]	$Z_{+/-}$	*d* [nm]
0.100	16.3	5.07
0.220	7.4	5.00
0.440	3.7	5.01
0.625	2.6	4.99
1.000	1.6	5.02

Materials and Methods

1. Lipid nanoparticle preparation

Cationic liquid crystalline nanoparticles (MO/DOMA/DOPE-PEG_{2000}, 82/15/3 mol.%) were prepared by hydration of a lyophilized mixed lipid film followed by vortex shaking, agitation by pulse sonication, and filtering through a Minisart High Flow filter (*Sartorius*). The investigated mixed film included the nonlamellar monoglyceride lipid 1-oleoyl-*rac*-glycerol (MO) (M_W 356.55, purity 99.5%, *Sigma*), the cationic amphiphile dioctadecyldimethylammonium bromide (DOMA) (M_W 630.95, purity ≥99.0%, Selectophore, *Fluka*), and the PEGyated lipid 1,2-dioleoyl-*sn*-glycero-3-phosphoethanolamine-*N*-(methoxy(polyethylene glycol)-2000) ammonium salt (DOPE-PEG_{2000}) (M_W 2801.51, purity ≥99.0%, *Avanti Polar Lipids*). The PEGylated lipid (DOPE-PEG_{2000}) was incorporated at a low molar percentage in order to preserve the nonlamellar inner structure of the nanocarriers. The hydration and dispersion of the lyophilized lipid film was performed in an excess phosphate buffer phase (NaH_2PO_4/Na_2HPO_4, 1.10^{-2}M, pH 7, p.a. grade, *Fluka*). The buffer solution was prepared using MilliQ water of resistivity 18.2 MΩ.cm (*Millipore Co*.). A ultrasonication ice bath (Branson 2510) was used for sample homogenization. Endotoxin-free plasmid DNA, encoding for human brain-derived neurotrophic factor (BDNF), was prepared by custom gene synthesis, subcloning, and purification (*GenScript Co*., NJ) using a cloning site of pEGFP-N1 (*Clontech*).

2. Synchrotron radiation small-angle X-ray scattering coupled to a rapid-mixing stopped-flow device

Small angle X-ray scattering experiments were performed at the ID02 beamline [9] of the European Synchrotron Radiation Facility (Grenoble, France). The time-resolved 2D SAXS patterns were recorded using a high-sensitivity low noise CCD detector (FReLoN 4M) having an active area of 100 mm x 100 mm which was divided into 512×512 pixels with 4×4 binning. The X-ray wavelength and sample-to-detector distance were 0.1 nm and 1.5 m, respectively corresponding to an accessible q-range of 0.07 to 3.2 nm^{-1}. The data acquisition sequence was hardware triggered by the stopped-flow device. Each SAXS pattern was integrated over 4 ms as defined by a tandem X-ray shutter and the readout time of the CCD detector was about 190 ms. The incident and transmitted beam intensities were recorded simultaneously with every SAXS frame. The dead time between the frames (~ 190 ms) was filled by means of a sequential data acquisition scheme in which the stopped-flow mixing sequences were repeated many times and the successive SAXS data acquisitions were progressively delayed in steps of 4 ms. This scheme allowed to check the kinetic

reproducibility and robustness of the data, and in addition avoided the radiation damage that would have been a serious problem in the case of continuous exposure to the X-ray beam (4.7×10^{13} photons/sec).

Mixing of equal volumes (100 μL) of supercoiled pDNA and PEGylated cationic lipid nanoparticles was performed by a stopped-flow apparatus SFM-400 (*Bio-Logic*, Claix, France). The scattering cell was fabricated from a quartz capillary (1.5 mm diameter, wall thickness 10 μm) and connected to the outlet of the last mixer. The reactant solutions were degassed and the test of the quality of mixing and calibration of stopped-flow dead time were performed by the method described elsewhere [10]. The flow time used for rapid mixing of the two components was 50 ms and during which the kinetic time is equal to the dead time of the stopped-flow device (~2.5 ms). The kinetic time evolved above this dead time upon cessation of the flow and the first 4 ms SAXS frame was acquired during the final phase of the flow corresponding to the earliest structural signal accessible. After each data acquisition sequence, the 2D images were corrected for dark current, detector spatial response function, etc. and normalized to absolute intensity unit. Normalized 2D patterns were subsequently azimuthally averaged to obtain the 1D scattering curves. Multiple patterns (20-30) of the scattering background from the quartz capillary and the solvent were measured and processed in the same way, averaged and subtracted from the time-resolved data using the *SAXS Utilities* software (www.sztucki.de/SAXSutilities/). Steady-state SAXS patterns were recorded using a flow-through capillary cell with data acquisition time of 100 ms.

3. SAXS data fitting and analysis

3.1. Scattering from a bicontinuous inverted cubic phase

The model of Clerc, Dubous-Violette, Garstecki and Hołyst [11,12] was used to determine the structural parameters of the double diamond inverted cubic lattice structure and the average water channel diameter, D_w. In this model, the lipid bilayer thickness, L, in the cubic lipid membrane is assumed to be a constant throughout. The intensity of the cubic phase peaks is given by:

$$I(q) = \frac{c_1}{q^2} \sum_{hkl} \exp\left[-\frac{(q - q_{hkl})^2}{2\sigma^2} \right] I_{hkl} \qquad (1),$$

where the peak positions are denoted by q_{hkl}, the peak widths for all peaks of the inverted cubic phase are considered to be the same and described by σ. The cubic phase individual peak intensities are given by I_{hkl}. The model scattering intensities are defined as

$$I_{hkl}(L) = M_{hkl}\left[F_{hkl}^{S*} \frac{\sin\left[\alpha_{hkl}\ \pi\ (h^2+k^2+l^2)^{1/2} L^*\right]}{\alpha_{hkl}\ 2\pi\ (h^2+k^2+l^2)^{1/2}} \right]^2 \qquad (2),$$

where $L^* = L/a$ is the dimensionless lipid layer thickness, a is the unit cell parameter, $F^{S}*_{hkl}$ is the dimensionless structure factor, M_{hkl} is a multiplicity factor, and α_{hkl} are correction parameters for a particular cubic lattice. Having done the fitting for L, the value of D_w was determined from the relationship $D_w = 0.707a - L$. Our nonlinear least-squares fitting algorithm is based on the well known Levenberg-Marquardt method.

3.2. Scattering from a core/shell cylinder

A model of a core/shell cylinder was used for fitting of the pDNA scattering curve:

$$P_{cyl}(q, \Delta\eta, R) = \frac{2\pi R^2 L \Delta\eta J_1(qR\sqrt{1-h^2})}{qR\sqrt{1-h^2}} \frac{\sin(qL_h/2)}{qL_h/2},$$

$$I_{cyl}(q) = \int_0^1 \left(P_{cyl}(q, \eta_{core} - \eta_{shell}, R) + P_{cyl}(q, \eta_{shell} - \eta_{sol}, R + \Delta R)\right)^2 dh .$$

Where R is the core radius, ΔR is the shell radius, $\eta_{core}, \eta_{shell}, \eta_{sol}$ are the core, shell and solvent contrasts. The length of the cylinder is L. J_1(x) is the first-order Bessel function of a first kind.

3.3. Pair distance distribution

The pair distance distribution function p(r) has been determined by GNOM [13] (http://www.embl-hamburg.de/biosaxs/gnom.html).

4. Cryogenic Transmission Electron Microscopy (Cryo-TEM)

For cryo-TEM imaging, liquid samples (2 µL) were dropped on a lacey carbon film covered copper grid (Science Services, Munich, Germany), which was hydrophilized by glow discharge for 15 s. The thin film specimens were instantly shock frozen by rapid immersion into liquid ethane and cooled to approximately 90 K by liquid nitrogen in a temperature-controlled freezing unit (Zeiss Cryobox, Zeiss NTS GmbH, Oberkochen, Germany). After removing ethane, the frozen samples were inserted into a cryo transfer holder (CT3500, Gatan, Munich, Germany) and transferred to a Zeiss EM922 Omega energy-filtered TEM (EFTEM) instrument (Zeiss NTS GmbH, Oberkochen, Germany). The imaging studies were carried out at temperatures around 90 K. The TEM instrument was operated at an acceleration

voltage of 200 kV. Zero-loss-filtered images (ΔE = 0 eV) were taken under reduced dose conditions (100-1000 e/nm^2). The images were recorded digitally by a bottom-mounted charge-coupled device (CCD) camera system (Ultra Scan 1000, Gatan, Munich, Germany) and combined and processed with a digital imaging processing system (Digital Micrograph GMS 1.8, Gatan, Munich, Germany).

5. Quasi-elastic light scattering (QELS)

The hydrodynamic diameter of the dispersed nanoparticle (NP) objects was determined by quasi-elastic light scattering using a Nanosizer aparatus (Nano-ZS90, *MALVERN*) at a scattering angle of 90° and at 25 °C. The mean hydrodynamic diameter, d_H, was calculated considering the average translational diffusion coefficient, D, of the particles in accordance with the Stokes-Einstein law for spherical particles in the absence of interactions: $d_H = k_BT/3\eta\pi D$, where k_B is the Boltzmann constant, T is temperature, and η is the viscosity of the aqueous medium. The size measurements were performed after dilution of 150µL of lipid NPs sample in 1 ml of phosphate buffer. Three measurements were averaged for each sample. The results were analyzed using the MALVERN Zetasizer software (version 6.11).

Supplementary discussion on Figure 3S and Table 1S

The rate constants of charge neutralization (k_1) have been estimated from non-structural, fluorescence and turbidity measurements [14], which lack direct information about the ultrastructures involved. Any structural intermediates related to this fast process, covering the 300 μsec to 3 ms time scale, were not accessed here as it fell in the range of the deadtime of the stopped-flow device (~2.5 ms). In case of significant structural modifications, by using slow flow rates of mixing, as well as low pDNA concentrations, one may render the pDNA neutralization step (referred to as "stage 1" of the complexation) experimentally more accessible.

The obtained d-spacing, $d \approx 5$ nm (Table 1S), implies that the studied nonlamellar lipid monoolein favours compact pDNA structures. The plasmids are accommodated as intercalated species in the interlayer aqueous compartments of about 2 nm thickness. The MO bilayer thickness has been determined to be $L = 3.2$ nm in single-component lipid assemblies [3], while the cationic lipid membrane thickness [15,16] has been in the range 3.5–3.9 nm. The hydrodynamic diameter of the investigated supercoiled pDNA, $d_H \approx 10$ nm, was determined in a fully hydrated state by QELS (Fig. 4S), whereas the diameter of the DNA double strand is around 2 nm. Hence, tight nearly anhydrous pDNA packing can be deduced from the structural data in Table 1S. For comparison, the multilamellar periodicity of lipid/DNA complexes, formed with lamellar lipids, is in the range of $d = 6.5$ nm – 8.0 nm; the thickness of the aqueous layer compartments [15,17] being larger ($d_w = 2.5$ nm – 2.6 nm) in such complexes. Therefore, the nanoconfinement of the neurotrophic plasmid and its charge neutralization by cationic cubic NPs lead to essential pDNA dehydration and compaction.

References

(1) Helgstrand, C.; Munshi, S.; Johnson, J.E.; Liljas, L. The Refined Structure of *Nudaurelia Capensis Omega Virus* Reveals Control Elements for a T = 4 Capsid Maturation. *Virology* **2004**, *318*, 192-203.

(2) Natarajan, P.; Lander, G.C.; Shepherd, C.M.; Reddy, V.S.; Brooks III, C.L.; Johnson, J.E. Exploring Icosahedral Virus Structures with VIPER. *Nat. Rev. Microbiol.* **2005***, 3*, 809-817.

(3) Angelova, A.; Angelov, B.; Lesieur, S.; Mutafchieva, R.; Ollivon, M.; Bourgaux, C.; Willumeit, R.; Couvreur, P. Dynamic Control of Nanofluidic Channels in Protein Drug Delivery Vehicles. *J. Drug Deliv. Sci. Tech*. **2008**, *18*, 41-45.

(4) Angelov, B.; Angelova, A.; Garamus, V.M.; Le Bas, G.; Lesieur, S.; Ollivon, M.; Funari, S.S.; Willumeit, R.; Couvreur P. Small-Angle Neutron and X-ray Scattering from Amphiphilic Stimuli-Responsive Diamond Type Bicontinuous Cubic Phase. *J. Am. Chem. Soc*. **2007**, *129,* 13474 -13479.

(5) Angelova, A.; Angelov, B.; Garamus, V.M.; Couvreur, P.; Lesieur, S. Small-angle X-ray Scattering Investigations of Biomolecular Confinement, Loading, and Release from Liquid Crystalline Nanochannel Assemblies. *J. Phys. Chem. Lett*. **2012**, *3*, 445-457.

(6) Angelov, B.; Angelova, A.; Garamus, V.M.; Drechsler, M.; Willumeit, R.; Mutafchieva, R.; Štěpánek, P.; Lesieur, S. Earliest Stage of the Tetrahedral Nanochannel Formation in Cubosome Particles from Unilamellar Nanovesicles. *Langmuir* **2012**, *28*, 16647–16655.

(7) Angelov, B.; Angelova, A.; Papahadjopoulos-Sternberg, B.; Hoffmann, S.V.; Nicolas, V.; Lesieur, S. Protein-Containing PEGylated Cubosomic Particles: Freeze-Fracture Electron Microscopy and Synchrotron Radiation Circular Dichroism Study. *J. Phys. Chem. B* **2012**, *116*, 7676-7686.

(8) Maltsev, E.; Wattis, J.; Byrne, H. DNA Charge Neutralization by Linear Polymers: Irreversible Binding. *Physical Review E* **2006**, *74*, 011904.

(9) Panine, P.; Finet, S.; Weiss, T. M.; Narayanan, T. Probing Fast Kinetics in Complex Fluids by Combined Rapid Mixing and Small-Angle X-ray Scattering. *Adv. Colloid Interface Sci.* **2006**, *127*, 9–18.

(10) Bressel, K.; Muthig, M.; Prevost, S.; Gummel, J.; Narayanan, T.; Gradzielski, M. Shaping Vesicles-Controlling Size and Stability by Admixture of Amphiphilic Copolymer. *ACS Nano* **2012**, *7*, 5858-5865.

(11) Clerc M.; Dubois-Violette, E. X-ray Scattering by Bicontinuous Cubic Phases. *J. Phys. II*, **1994**, *4*, 275-286.

(12) Garstecki, P; Holyst, R. Scattering Patterns of Self-Assembled Cubic Phases. II. Analysis of the Experimental Spectra. *Langmuir* **2002**, *18*, 2529–2537.

(13) Svergun, D.I. Determination of the Regularization Parameter in Indirect-Transform Methods using Perceptual Criteria. *J. Appl. Cryst.* **1992**, *25*, 495-503.

(14) Barreleiro, P.C.; Lindman, B. The Kinetics of DNA-Cationic Vesicle Complex Formation. *J. Phys. Chem. B* **2003**, *107*, 6208-6213.

(15) Schmutz, M.; Durand, D.; Debin, A.; Palvadeau, Y.; Etienne, A.; Thierry, A.R. DNA Packing in Stable Lipid Complexes Designed for Gene Transfer Imitates DNA Compaction in Bacteriophage. *Proc. Nat. Acad. Sci*. **1999**, *96*, 12293–12298.

(16) Saveyn, P.; van der Meeren, P.; Zackrisson, M.; Narayanan, T.; Olsson, U. Subgel Transition in Diluted Vesicular DODAB Dispersions. *Soft Matter* **2009**, *5*, 1735–1742.

(17) Barreleiro, P.C.A.; May, R.P.; Lindman, B. Mechanism of Formation of DNA–Cationic Vesicle Complexes. *Faraday Discuss.* **2002**, *122*, 191–201.